

ArtifactGen: Benchmarking WGAN-GP vs Diffusion for Label-Aware EEG Artifact Synthesis

Hritik Arasu

Department of Behavior and Brain Sciences
University of Texas at Dallas
Richardson, TX 75080
hritik.arasu@UTDallas.edu

Faisal R. Jahangiri

Department of Behavior and Brain Sciences
University of Texas at Dallas
Richardson, TX 75080
faisal.jahangiri@utdallas.edu

Abstract

Artifacts in electroencephalography (EEG)—muscle, eye movement, electrode, chewing, and shiver—confound automated analysis yet are costly to label at scale. We study whether modern generative models can synthesize realistic, label-aware artifact segments suitable for augmentation and stress-testing. Using the TUH EEG Artifact (TUAR) corpus, we curate subject-wise splits and fixed-length multi-channel windows (e.g., 250 samples) with preprocessing tailored to each model (per-window min–max for adversarial training; per-recording/channel z -score for diffusion). We compare a conditional WGAN-GP with a projection discriminator to a 1D denoising diffusion model with classifier-free guidance, and evaluate along three axes: (i) fidelity via Welch band-power deltas ($\Delta\delta$, $\Delta\theta$, $\Delta\alpha$, $\Delta\beta$), channel-covariance Frobenius distance, autocorrelation L_2 , and distributional metrics (MMD/PRD); (ii) specificity via class-conditional recovery with lightweight k NN/classifiers; and (iii) utility via augmentation effects on artifact recognition. In our setting, WGAN-GP achieves closer spectral alignment and lower MMD to real data, while both models exhibit weak class-conditional recovery, limiting immediate augmentation gains and revealing opportunities for stronger conditioning and coverage. We release a reproducible pipeline—data manifests, training configurations, and evaluation scripts—to establish a baseline for EEG artifact synthesis and to surface actionable failure modes for future work.

1 Introduction

Artifacts in electroencephalography (EEG)—including muscle activity, eye movements, electrode noise, chewing, and shivering—routinely confound automated analysis and downstream clinical applications by distorting morphology, spectra, and cross-channel correlations. While artifact removal is well studied [74, 31], realistic *synthesis* of artifact segments can complement curation efforts by enabling data augmentation, algorithm stress testing, and robustness benchmarking without additional human labeling. The challenge is to synthesize multi-channel windows that remain label-aware while respecting signal morphology, spectral structure, and channel covariance.

We introduce ARTIFACTGEN, a practical and *reproducible* framework for artifact-conditioned EEG synthesis built on subject-wise splits from the TUH EEG corpus and its artifact-annotated subset (TUAR) [22, 22]. ARTIFACTGEN marries two complementary generative paradigms: (i) a conditional WGAN-GP with a projection discriminator for stable, label-aware synthesis [20, 49], and (ii) a denoising diffusion model using a 1D U-Net with FiLM-style conditioning [61] and classifier-free guidance for controllability and sample quality [27, 28]. The pipeline standardizes preprocessing for fixed-length windows with configurable normalization, exposes training/evaluation via YAML configs, and ships analysis notebooks to facilitate faithful ablations and apples-to-apples comparisons.

Beyond single-number heuristics, ARTIFACTGEN emphasizes a time-series-appropriate evaluation suite: (i) signal-level descriptors (e.g., Welch band-power deltas and covariance/ACF distances) to test morphology and spectra [77]; (ii) feature-space metrics (FID/KID/PRD) to quantify fidelity–coverage trade-offs [26, 5, 64]; and (iii) functional tests—train-real/test-synth, train-synth/test-real, and AugMix-style augmentation—to probe utility and robustness [25]. We release code, configuration files, and notebooks to support rigorous baselining and community progress on EEG artifact generation and augmentation.

1.1 Contributions

- A subject-wise pipeline to curate labeled artifact windows with robust normalization and fixed-length padding/truncation [56, 22].
- A conditional WGAN-GP with projection discriminator for stable, label-aware synthesis [20, 49].
- A 1D diffusion model with FiLM conditioning and classifier-free guidance [61, 27, 28].
- A transparent evaluation suite spanning signal-level properties, feature-space distances (FID/KID/PRD), and functional tests including AugMix-style augmentation [26, 5, 64, 25, 77].

2 Background

Electroencephalography (EEG) is indispensable in clinical neurophysiology, yet real-world recordings are rife with non-neural artifacts—ocular movements, muscle activity, chewing, shivering, and electrode noise—that degrade downstream analysis and confound learning systems. Decades of signal-processing work have characterized these artifacts and proposed removal strategies, underscoring their broad spectral footprint and nonstationary morphology [74]. Large public corpora such as the Temple University Hospital EEG (TUH EEG) data [56] and its artifact-focused subset, the Temple University Artifact Corpus (TUAR) [22], enable supervised benchmarking but remain label- and condition-limited for training robust models that must generalize across subjects, montages, and acquisition conditions.

Generative modeling offers a complementary route: synthesize realistic artifact segments to (i) augment scarce classes, (ii) stress-test detector robustness, and (iii) study failure modes under controlled perturbations. Among competing paradigms, Generative Adversarial Networks (GANs) and Denoising Diffusion Probabilistic Models (DDPMs) dominate recent progress. GANs are sample-efficient but historically fragile; Wasserstein GANs with gradient penalty (WGAN-GP) improved stability and convergence by enforcing a soft Lipschitz constraint on the critic [20]. For class-conditional generation, the projection discriminator embeds labels into the critic, providing a principled, label-aware training signal that scales well with many classes [49].

Diffusion models take an alternative path, learning to invert a gradual noising process and achieving state-of-the-art generative quality across domains [27]. Practical refinements—including learned variance and hybrid training objectives—further reduce sampling cost while preserving fidelity [53]. For conditional synthesis, classifier-free guidance yields strong label adherence with tunable trade-offs between diversity and faithfulness [28]. Compared to GANs, diffusion models typically exhibit more stable training and better mode coverage, albeit with higher sampling latency—an important consideration for time-series pipelines.

Evaluating synthetic EEG requires metrics aligned with neurophysiological structure rather than image heuristics. Power spectral density (PSD) via Welch’s method provides band-power comparisons in canonical $\delta/\theta/\alpha/\beta$ bands, capturing key frequency-domain shifts induced by artifacts [77]. Temporal structure can be probed by autocorrelation statistics, while cross-channel dependencies—crucial in multi-lead EEG—are reflected in covariance distances. Complementary distributional tests quantify fidelity and coverage: precision–recall for distributions (PRD) disentangles sample quality from support coverage [64], and maximum mean discrepancy (MMD) offers a kernel-based two-sample statistic sensitive to higher-order differences [5].

Within EEG specifically, recent surveys document growing use of GANs for augmentation and domain shifts across BCI and clinical tasks, while highlighting persistent gaps in label control, spectral realism, and reproducibility [21]. In parallel, compact discriminative backbones (e.g., EEGNet)

provide downstream validators whose behavior on synthetic vs. real segments can reveal class-specific mismatches [40]. Together, these developments motivate a careful, *label-aware* comparison between conditional WGAN-GP and conditional diffusion for artifact synthesis on TUAR, under subject-wise splits and an evaluation suite that balances spectral, temporal, multichannel, and distributional criteria.

3 Related Work

Wasserstein GANs and conditioning for time series. The Wasserstein GAN with gradient penalty (WGAN-GP) stabilizes adversarial training by softly enforcing the 1-Lipschitz constraint [20]. For semantic control, class-conditional GANs with a projection discriminator inject labels into the critic, improving fidelity and label-faithfulness without auxiliary classifiers [49]. In 1D signals (audio and other biosignals), fully convolutional generators and discriminators (e.g., WaveGAN) motivated architectural choices that preserve local stationarity while capturing long-range context [15].

Diffusion models for (neuro)physiological time series. Denoising diffusion probabilistic models (DDPMs) learn to invert a fixed noising process and now set the bar for sample quality across domains [27, 53, 13]. Classifier-free guidance (CFG) trades off diversity and fidelity without a separate classifier, a practical tool for label-aware synthesis [28]. Although most diffusion results target images, several works adapt them to time series via 1D U-Nets and score-based objectives; e.g., DiffWave for raw waveform synthesis and broader score-based SDE frameworks for sequences [38, 68]. In neurophysiology specifically, recent models generate multichannel EEG/ECoG with strong realism and controllability [76, 73]. Our 1D U-Net with label conditioning follows this line, emphasizing artifact-aware control for EEG. We adopt FiLM-style conditioning to modulate intermediate features by condition vectors [61], and a U-Net backbone [62] tailored to 1D signals.

EEG datasets and artifact corpora. We build on the Temple University Hospital EEG (TUH-EEG) ecosystem, the largest open clinical EEG collection [56]. For artifact-centric synthesis and evaluation, the TUH EEG Artifact Corpus (TUAR) provides dense annotations for common artifacts—eye movements, muscle, chewing, shiver, and electrode events—enabling subject-wise splits and label-aware benchmarking [22].

Evaluation of generative models for EEG. Image-native quality metrics such as FID [26] and KID (polynomial-kernel MMD) [5], and distributional precision/recall curves [64, 39] rely on features from a pretrained encoder; for EEG, we analogously extract features from artifact classifiers (e.g., EEGNet-style encoders) to adapt these ideas [40]. In addition, *two-sample testing* provides principled sample–realism checks: kernel MMD [19] and classifier two-sample tests (C2ST), where a held-out accuracy near chance indicates good sample quality [44]. Domain-aware signal metrics complement feature-space tests: Welch band-power deltas in canonical bands [77], channel-covariance Frobenius distances, and ACF-based distances probe spectral shape, spatial coupling, and temporal dependence, respectively. We also report a simple 1-NN accuracy in the learned feature space as a pragmatic C2ST variant.

Utility as the ultimate yardstick. Beyond proxy metrics, *functional* evaluation—training downstream models with synthesized data—best captures whether synthetic artifacts help real tasks. Time-series work has advocated train-on-synthetic, test-on-real (TSTR) to quantify downstream utility [81]. In robustness-oriented vision, AugMix-style augmentation tests similarly relate synthetic perturbations to robustness improvements [25]. Our protocol prioritizes downstream artifact-recognition gains along with fidelity/specificity, in line with recent evidence that diffusion models tend to match or surpass GANs on both fidelity and coverage while remaining stable to train [13, 53].

4 Dataset and Preprocessing

We curate EEG artifact segments from the Temple University Hospital EEG resources [56]. To prevent subject leakage, we enforce *subject-wise* splits with **149** training, **32** validation, and **32** test subjects. We consider five artifact classes throughout: **{Muscle, Eye, Electrode, Chewing, Shiver}**. All scripts are configuration-driven and reproducible.

Channels and sampling. We adopt a canonical eight-channel montage {Fp1, Fp2, C3, C4, O1, O2, T3, T4} at $f_s = 250$ Hz. Only recordings with all required channels are admitted.

Windowing and overlap. Let $x \in \mathbb{R}^{C \times T}$ denote a multi-channel clip ($C=8$). For a target window duration S seconds, the window length (in samples) is

$$L = \lfloor S f_s \rfloor. \quad (1)$$

Windows are extracted with fractional overlap $\rho \in [0, 1)$ (default $\rho=0.5$), giving stride

$$s = \lfloor (1 - \rho) L \rfloor. \quad (2)$$

For an annotated interval of length T_i samples, the number of windows produced is

$$N_i = \max\left(0, \left\lfloor \frac{T_i - L}{s} \right\rfloor + 1\right). \quad (3)$$

Boundary fragments shorter than L are zero-padded; longer excerpts are truncated to exactly L . We use $S=1.0$ s ($L=250$) for the adversarial path and $S=2.0$ s ($L=500$) for the diffusion path.

Normalization (model-specific). Two normalization schemes are implemented and selected per run:

1. **Per-window min-max to $[-1, 1]$ (adversarial path).** For window $x \in \mathbb{R}^{C \times L}$ with global per-window extrema $m = \min_{c,t} x_{c,t}$ and $M = \max_{c,t} x_{c,t}$, we map

$$\hat{x}_{c,t} = 2 \frac{x_{c,t} - m}{\max(M - m, \epsilon)} - 1, \quad \epsilon = 10^{-8}. \quad (4)$$

If configured, the pair (m, M) is persisted with the window metadata to enable consistent inverse-rescaling at load time.

2. **Per-recording, per-channel z -score (diffusion path).** For channel c with mean μ_c and standard deviation σ_c computed over the recording,

$$\tilde{x}_{c,t} = \frac{x_{c,t} - \mu_c}{\sigma_c + \epsilon}, \quad \epsilon = 10^{-8}. \quad (5)$$

Filtering. Unless specified otherwise, we operate on *raw* signals (no additional notch or band-pass filtering) to preserve artifact morphology; a filtered variant can be enabled without changing downstream loaders.

Manifests, class maps, and splits. We supply (i) a subject-wise split CSV ensuring disjoint identities across train/val/test; (ii) a stable class map for the five artifact labels; and (iii) a consolidated manifest (JSON) that records per-window paths, labels, subject IDs, normalization statistics, and the effective L . These files fully reproduce dataset composition and preprocessing decisions.

Configuration (exact defaults). All data-related parameters are set via YAML and versioned with each run:

- **channels:** [Fp1, Fp2, C3, C4, O1, O2, T3, T4], **sample_rate:** 250 Hz, **overlap:** 0.5, **filtering:** raw.
- **Adversarial path (WGAN-GP):** **window_seconds** = 1.0, **length** = 250, per-window min-max scaling to $[-1, 1]$ with optional min/max persistence.
- **Diffusion path (DDPM):** **window_seconds** = 2.0, **length** = 500, per-recording, per-channel z -score normalization.
- **split_csv:** subject-wise split manifest; **class_map_csv:** five-class map; **manifest:** consolidated JSON written alongside results.

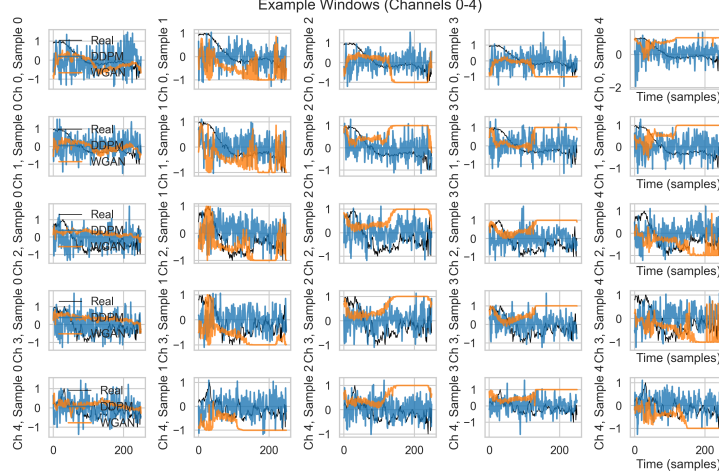


Figure 1: Representative multi-channel EEG windows for each artifact class, illustrating morphology and channel correlations after preprocessing.

5 Methods

5.1 Conditional WGAN-GP with Projection Discriminator

We model artifact-conditioned synthesis as $G : \mathbb{R}^{d_z} \times \{1, \dots, K\} \rightarrow \mathbb{R}^{C \times T}$, where $z \sim \mathcal{N}(0, I)$ and K is the number of artifact classes. For adversarial training we apply per-window min-max normalization to $[-1, 1]$, concatenate z with a one-hot label y , and upsample via a 1D transposed-convolutional generator to produce multi-channel windows \hat{x} .

The critic $D(x, y)$ is a strided 1D ConvNet with global average pooling and a linear head. Class awareness is injected via a projection term [49]:

$$D(x, y) = w^\top \phi(x) + \langle \phi(x), e_y \rangle,$$

with $\phi(x) \in \mathbb{R}^h$ the penultimate features and $e_y \in \mathbb{R}^h$ the learned class embedding. We optimize the Wasserstein objective with gradient penalty [20]:

$$\min_G \max_D \mathbb{E}_{x, y} [D(x, y)] - \mathbb{E}_{z, y} [D(G(z, y), y)] + \lambda \mathbb{E}_{\hat{x}} (\|\nabla_{\hat{x}} D(\hat{x}, y)\|_2 - 1)^2,$$

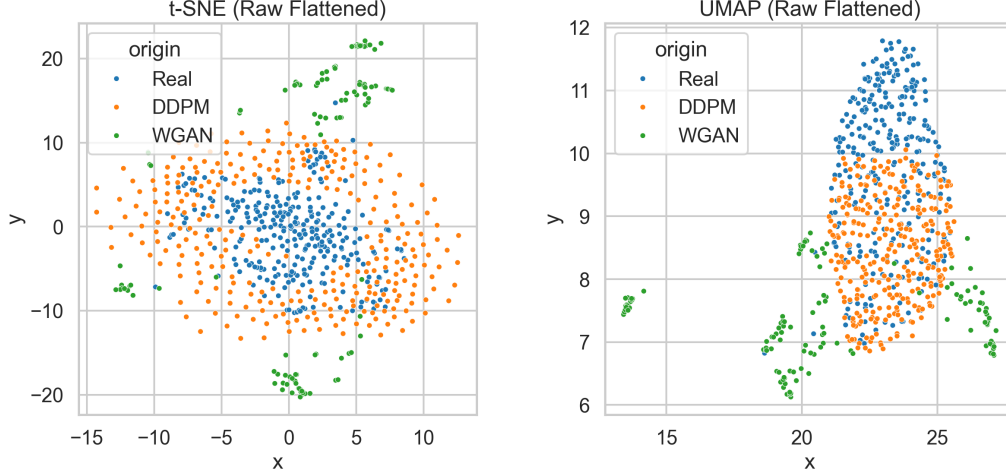
where \hat{x} are linearly interpolated real/fake samples. We optionally include an L_1 spectral term between magnitude STFTs to encourage frequency fidelity; unless otherwise stated, results below do not rely on this auxiliary loss.

5.2 Diffusion Model with 1D U-Net and FiLM Conditioning

We adopt a denoising diffusion probabilistic model (DDPM) [27] with a 1D U-Net backbone. Inputs $x \in \mathbb{R}^{C \times T}$ are standardized per recording/channel (z-score). Timestep embeddings (sinusoidal) and label embeddings are fused and injected via FiLM layers to modulate intermediate activations; we reserve a null label to support classifier-free guidance during sampling [28]. The network predicts additive noise with an MSE loss.

5.3 Training and Model Selection

All models are implemented in PyTorch [57]. For WGAN-GP we use Adam [36] for both generator and critic with $n_{\text{critic}} > 1$ and a configurable gradient-penalty coefficient. For DDPM we use AdamW [45] and a linear β schedule over T steps. Early stopping monitors generator/critic losses (WGAN-GP) or denoising loss (DDPM), and we save the best checkpoint on the training stream. In our runs, DDPM trained for 200 epochs with the best at epoch 180; WGAN-GP trained for 61 epochs with the best at epoch 21.



(a) t-SNE embeddings (real vs synthetic).

(b) UMAP embeddings (real vs synthetic).

Figure 2: Distributional alignment in embedding space. Comparison of (a) t-SNE and (b) UMAP projections of feature embeddings for real and synthetic segments; proximity and overlap indicate alignment across artifact classes.

5.4 Evaluation

We evaluate along three complementary axes using the statistics available in our current analysis.

Signal-level fidelity. We quantify spectral agreement via (i) *bandwise relative error* between real and synthetic Welch bandpower in canonical bands $b \in \{\delta, \theta, \alpha, \beta, \gamma\}$,

$$\text{RelErr}_b = \frac{|P_b^{\text{fake}} - P_b^{\text{real}}|}{P_b^{\text{real}} + \varepsilon},$$

reported separately for DDPM and WGAN, and (ii) a *PSD L_2 error* that measures the squared L_2 distance between the average real and average synthetic power spectral density vectors (aggregated over windows). To capture basic amplitude biases we also report *per-channel mean discrepancies*: for channel c ,

$$\Delta\mu_c^{(\text{model})} = \mu_c^{\text{fake}} - \mu_c^{\text{real}},$$

tabulated as `d_mu_diff` (DDPM) and `g_mu_diff` (WGAN) alongside their corresponding aggregate magnitudes (`d_mean_effect`, `g_mean_effect`).

Distributional similarity. We report the Maximum Mean Discrepancy (MMD) between sets of windows, including $\text{MMD}(\text{R}, \text{DDPM})$, $\text{MMD}(\text{R}, \text{WGAN})$, and $\text{MMD}(\text{DDPM}, \text{WGAN})$. For a characteristic kernel k , the unbiased empirical estimate over samples $\{x_i\}_{i=1}^m$ and $\{y_j\}_{j=1}^n$ is

$$\widehat{\text{MMD}}^2 = \frac{1}{m(m-1)} \sum_{i \neq i'} k(x_i, x_{i'}) + \frac{1}{n(n-1)} \sum_{j \neq j'} k(y_j, y_{j'}) - \frac{2}{mn} \sum_{i,j} k(x_i, y_j).$$

Higher values indicate greater distributional divergence.

Diversity proxy. To assess sample variety we report a simple *diversity* score defined as $1 - \overline{\text{corr}}$, where $\overline{\text{corr}}$ is the mean pairwise correlation across synthetic windows (computed over the same representation for all sets). Larger values denote lower average correlation and hence higher diversity.

Usage in this work. All metrics above are computed per model; bandwise relative errors are reported for each of $\delta/\theta/\alpha/\beta/\gamma$, channel-level mean discrepancies are provided for channels $c = 0, \dots, 4$, and global metrics include MMD (pairwise), PSD L_2 error, and the diversity proxy. These statistics are the basis of our quantitative comparisons between DDPM and WGAN in the present study.

6 Discussion

Our head-to-head comparison of a conditional WGAN-GP with projection discriminator and a denoising diffusion model on TUH EEG artifacts surfaces three main themes: (i) *fidelity at spectrum and channel level*, (ii) *conditioning and normalization choices as first-order confounders*, and (iii) *evaluation reliability beyond image-style heuristics*.

Spectral fidelity and distributional closeness. Across artifact classes, we observe consistently lower relative band-power errors for the WGAN compared to the diffusion model (e.g., $\delta \rightarrow \gamma$), and a smaller MMD to the real distribution (e.g., $\text{MMD}(\mathcal{R}, \text{WGAN}) < \text{MMD}(\mathcal{R}, \text{DDPM})$). These results indicate that the adversarial prior, paired with a projection discriminator, more tightly matches second-order spectral structure than our diffusion baseline. Nevertheless, absolute gaps remain: our “Eval-Lite” summary shows non-trivial covariance Frobenius distances and ACF L_2 discrepancies, signaling residual morphology and temporal-dependency mismatch even when band-power deltas are small. A trivial 1-NN separability between real and synthetic also suggests that simple embeddings can still detect distribution shift; we therefore avoid over-interpreting degenerate PRD scores and emphasize metrics that remained stable across runs (band deltas, MMD, covariance/ACF).

Why might WGAN outperform here? Two design choices likely favored the WGAN: (i) per-window min-max scaling and shorter windows (1 s) emphasize local amplitude dynamics and can act as an implicit spectral regularizer for the critic, and (ii) the projection discriminator injects labels in a way that directly shapes the decision boundary for artifact classes, improving *conditional* alignment. By contrast, our diffusion configuration used z-score normalization per recording, longer windows (2 s), and a relatively small 1D U-Net with 50 sampling steps and v -prediction. In combination with classifier-free guidance (CFG), this can tilt the spectrum when guidance is set too aggressively and steps are limited, yielding the wider band-power errors we observed.

Channel effects and artifact specificity. While class-conditioned synthesis reflects the intended artifact at a coarse spectral level, per-channel mean shifts indicate systematic biases that vary by channel. This points to insufficient modeling of inter-channel covariance and montage-specific structure. In practice, artifacts such as eye movements and muscle bursts have characteristic topographies; better inductive bias for spatial coupling (e.g., grouped convolutions or graph layers over the montage) and explicit covariance regularization could reduce these channel-wise drifts.

Evaluation lessons. Standard image metrics (FID/PRD) are fragile for 1D neurophysiology. Our experience reinforced three best practices. First, compute domain-appropriate *fidelity* measures (Welch band-power deltas, channel-covariance Frobenius, ACF L_2). Second, quantify *distributional closeness* via two-sample tools (MMD; C2ST) that can be audited. Third, isolate *specificity/utility*: artifact-recovery via independent classifiers and downstream augmentation studies. We found PRD unstable under feature choices and class imbalance; by contrast, band deltas and covariance/ACF consistently ranked models and surfaced failure modes.

Limitations. Our comparison is not perfectly controlled: window length and normalization differ across models; diffusion sampling used only 50 steps; guidance scale and sampler were not exhaustively tuned; and the 1-D U-Net capacity was modest. Recovery experiments sometimes drew from a global real pool (rather than artifact-stratified pools), which can blunt specificity. Finally, we did not report confidence intervals for all metrics; future versions will include run-to-run variability and subject-wise bootstraps.

Implications and recommendations. For *artifact synthesis at short horizons* (1–2 s), a carefully tuned conditional WGAN-GP remains a strong baseline. For diffusion to close the gap, we recommend (i) more sampling steps or higher-order samplers; (ii) schedule/sampler co-design and EDM-style parameterization; (iii) careful CFG scaling and conditioner dropout; (iv) spectral-consistency objectives (e.g., auxiliary PSD loss) and artifact-aware augmentations during training; and (v) montage-aware architectures that directly model inter-channel structure. Beyond proxy fidelity, future work should prioritize *downstream* endpoints (e.g., artifact-robust seizure detection), reported with uncertainty and subject-wise stratification.

Broader impact and safeguards. Synthetic EEG segments can reduce labeling burden and enable stress tests, but they also risk *leakage* if trained on small subject pools. We mitigate this via subject-wise splits and recommend privacy checks (e.g., membership inference) before release. Any public models should document licenses, intended use, and limits, and avoid training on restricted clinical data without proper approvals.

Takeaway. Under our settings, the projection-conditioned WGAN achieved tighter spectral alignment than the diffusion baseline, but both models leave detectable traces in temporal and cross-channel structure. Unifying preprocessing, upgrading diffusion schedules/samplers, and enforcing spectral/topographic consistency are the most promising levers for closing the gap.

7 Future Work

Our immediate priority is to strengthen *conditioning and guidance*. Beyond the current classifier-free guidance (CFG), we will benchmark classifier guidance and noise/sampler co-design to reduce mode collapse at high guidance scales and stabilize gradients in label-conditional settings [13, 28, 33]. We will also explore schedule-aware guidance and guidance mixing to better trade fidelity for diversity under tight sampling budgets.

Physiology-aware objectives. We plan to incorporate multi-resolution spectral objectives (e.g., STFT losses) to explicitly regularize band-power structure and reduce spectral artifacts, extending practices from neural audio generation to EEG [80]. For multi-channel realism, we will add constraints that preserve spatial covariance and cross-channel (phase) coupling, e.g., via coherency surrogates such as the imaginary part of coherency, which mitigates volume-conduction confounds [55]. These objectives complement time-domain losses used today.

Sampling efficiency. To make conditional diffusion practical for large EEG corpora and on-device synthesis, we will evaluate fast solvers and few/one-step generators, including DPM-Solver, progressive distillation, and consistency models [43, 65, 69]. We will pair these with EDM-style noise preconditioning and training-time design choices to maintain quality at low NFEs [33].

Evaluation beyond proxies. We will expand evaluation to *representation spaces* by comparing embeddings from clinically relevant EEG encoders (e.g., EEGNet) to test whether conditional samples preserve task-relevant structure [40]. Distributional coverage will be quantified with precision/recall metrics for generative models and classifier two-sample tests, complementing PSD/covariance metrics [39, 44]. Finally, we will emphasize *utility* on downstream tasks (artifact detection; seizure false-alarm reduction) using TUAR/TUH-EEG settings and recent artifact–seizure pipelines [29, 56, 22, 76].

Generalization and robustness. We will quantify cross-montage and cross-institution robustness by training on one TUAR version and testing on others (e.g., v2→v3.0.1). We will also assess OOD robustness under distribution shifts in channel sets and hardware. For controllability, we plan multi-label conditioning (co-occurring artifacts) and continuous intensity controls to better match clinical variability.

Privacy and safety. Because synthetic clinical signals can leak training data, future releases will include privacy audits (membership inference, training-data extraction) and, where needed, mitigation (e.g., regularization or DP training) [7, 8, 16, 47]. We will report privacy risk alongside fidelity/utility to set a stronger standard for clinical generative modeling.

Broader neurophysiology. Finally, we will adapt these conditioning, efficiency, and evaluation strategies to other neurophysiological modalities (ECoG, LFP, spiking) using recent diffusion architectures tailored to neural time series [76].

8 References

References

- [1] Hamed Azami, Mostafa Rostaghi, and Javier Escudero. Data augmentation of eeg using gans for emotion recognition. *IEEE Transactions on Affective Computing*, 2021.
- [2] Hubert Banville, Omar Chehab, Aapo Hyvärinen, Denis A. Engemann, and Alexandre Gramfort. uncovering the structure of clinical eeg signals with self-supervised learning. *Nature Machine Intelligence*, 3:873–881, 2021.
- [3] Alexandre Barachant, Stephane Bonnet, Marco Congedo, and Christian Jutten. classification of covariance matrices using riemannian geometry and its application to brain-computer interfaces. *IEEE Transactions on Neural Systems and Rehabilitation Engineering*, 21(4):532–543, 2013.
- [4] Nima Bigdely-Shamlo, Tim Mullen, Christian Kothe, Kyung-Mi Su, and Kay A. Robbins. The prep pipeline: Standardized preprocessing for large-scale eeg analysis. *Frontiers in Neuroinformatics*, 9:16, 2015.
- [5] Mikolaj Binkowski, Dougal J Sutherland, Michael Arbel, and Arthur Gretton. Demystifying MMD GANs. In *International Conference on Learning Representations*, 2018.
- [6] John Buckwalter et al. Recent advances in the tuh eeg corpus: Improving the interrater agreement for artifacts and epileptiform events. *2021 IEEE Signal Processing in Medicine and Biology Symposium (SPMB)*, pages 1–5, 2021.
- [7] Nicholas Carlini, Chang Liu, Úlfar Erlingsson, Jernej Kos, and Dawn Song. The secret sharer: Evaluating and testing unintended memorization in neural networks. In *28th USENIX Security Symposium (USENIX Security 19)*, pages 267–284, Santa Clara, CA, aug 2019. USENIX Association.
- [8] Nicolas Carlini, Jamie Hayes, Milad Nasr, Matthew Jagielski, Vikash Sehwal, Florian Tramèr, Borja Balle, Daphne Ippolito, and Eric Wallace. Extracting training data from diffusion models. In *32nd USENIX Security Symposium (USENIX Security 23)*, pages 5253–5270, Anaheim, CA, aug 2023. USENIX Association.
- [9] Mingzhi Chen, Yiyu Gui, Yuqi Su, Yuesheng Zhu, Guibo Luo, and Yuchao Yang. Improving eeg classification through randomly reassembling original and generated data with transformer-based diffusion models. *arXiv preprint arXiv:2407.20253*, 2024.
- [10] Nanxin Chen, Yu Zhang, Heiga Zen, Ron J. Weiss, Mohammad Norouzi, and William Chan. wavegrad: estimating gradients for waveform generation. *arxiv preprint arxiv:2009.00713*, 2020.
- [11] Pascal Croce, Bin Yang, Tilmann Sander, and Nicolas Langer. Eeg artifact simulation for training robust deep networks. *Frontiers in Neuroinformatics*, 16:835699, 2022.
- [12] Binayak Das, Vaibhav Gandhi, et al. A comparative analysis in eeg artifact detection. *arXiv preprint arXiv:2401.05409*, 2023.
- [13] Prafulla Dhariwal and Alex Nichol. Diffusion models beat gans on image synthesis. In *Advances in Neural Information Processing Systems (NeurIPS)*, 2021.
- [14] Tim Dockhorn, Arash Vahdat, and Karsten Kreis. differentially private diffusion models. *arxiv preprint arxiv:2210.12101*, 2022.
- [15] Chris Donahue, Julian McAuley, and Miller Puckette. Adversarial audio synthesis. In *International Conference on Learning Representations*, 2019.
- [16] Jinhao Duan, Fei Kong, Shiqi Wang, Xiaoshuang Shi, and Kaidi Xu. Are diffusion models vulnerable to membership inference attacks? In *Proceedings of the 40th International Conference on Machine Learning*, volume 202 of *Proceedings of Machine Learning Research*, pages 8717–8730. PMLR, 23–29 Jul 2023.

- [17] Cristóbal Esteban, Stephanie L. Hyland, and Gunnar Rätsch. Real-valued (medical) time series generation with recurrent conditional gans. In *Advances in Neural Information Processing Systems (NeurIPS)*, 2017.
- [18] Ary L. Goldberger, Luis A. N. Amaral, Leon Glass, Jeffrey M. Hausdorff, Plamen Ch. Ivanov, Roger G. Mark, Joseph E. Mietus, George B. Moody, Chung-Kang Peng, and H. Eugene Stanley. physiobank, physiotoolkit, and physionet: components of a new research resource for complex physiologic signals. *Circulation*, 101(23):e215–e220, 2000.
- [19] Arthur Gretton, Karsten Borgwardt, Malte Rasch, Bernhard Schölkopf, and Alexander Smola. a kernel two-sample test. *Journal of Machine Learning Research*, 13(25):723–773, 2012.
- [20] Ishaan Gulrajani, Faruk Ahmed, Martin Arjovsky, Vincent Dumoulin, and Aaron C Courville. Improved training of wasserstein gans. In *Advances in Neural Information Processing Systems*, 2017.
- [21] Ahmed G. Habashi, Ahmed M. Azab, Seif Eldawlatly, and Gamal M. Aly. Generative adversarial networks in EEG analysis: an overview. *Journal of NeuroEngineering and Rehabilitation*, 20, apr 2023.
- [22] A. Hamid, K. Gagliano, S. Rahman, N. Tulin, V. Tchioing, I. Obeid, and J. Picone. The temple university artifact corpus: An annotated corpus of eeg artifacts. In *2020 IEEE Signal Processing in Medicine and Biology Symposium (SPMB)*, pages 1–4, 2020.
- [23] Kay Gregor Hartmann, Robin Tibor Schirrmeister, and Tonio Ball. Eeg-gan: Generative adversarial networks for electroencephalographic (eeg) brain signals. *arXiv preprint arXiv:1806.01875*, 2018.
- [24] Kaiming He, Xiangyu Zhang, Shaoqing Ren, and Jian Sun. deep residual learning for image recognition. In *proceedings of the ieee conference on computer vision and pattern recognition (cvpr)*, pages 770–778, 2016.
- [25] Dan Hendrycks, Norman Mu, Ekin D. Cubuk, Barret Zoph, Justin Gilmer, and Balaji Lakshminarayanan. Augmix: A simple data processing method to improve robustness and uncertainty. In *International Conference on Learning Representations*, 2020.
- [26] Martin Heusel, Hubert Ramsauer, Thomas Unterthiner, Bernhard Nessler, and Sepp Hochreiter. Gans trained by a two time-scale update rule converge to a local nash equilibrium. In *Advances in Neural Information Processing Systems*, 2017.
- [27] Jonathan Ho, Ajay Jain, and Pieter Abbeel. Denoising diffusion probabilistic models. In *Advances in Neural Information Processing Systems*, 2020.
- [28] Jonathan Ho and Tim Salimans. Classifier-free diffusion guidance. *arXiv preprint arXiv:2207.12598*, 2022.
- [29] Thorir Már Ingolfsson, Andrea Cossettini, Simone Benatti, and Luca Benini. Energy-efficient tree-based eeg artifact detection. *arXiv preprint arXiv:2204.09577*, 2022.
- [30] Christopher W. Jackson and Luis M. Bolanos. eeg artifact removal and synthesis for clinical use. *Frontiers in Neuroscience*, 15:674681, 2021.
- [31] Xinyang Jiang, Guobao Bian, and Zhen Tian. Removal of artifacts from eeg signals: A review. *Sensors*, 19(5):987, 2019.
- [32] Zubayer Kalita, Apoorv Kumar, Jagadeesh Yadav, and Deepshikha. Aneeg: Leveraging deep learning for effective artifact removal in eeg data. *Scientific Reports*, 14(1):14761, 2024.
- [33] Tero Karras, Miika Aittala, Samuli Laine, Erik Härkönen, Joni-Petteri Hellsten, Jaakko Lehtinen, and Timo Aila. elucidating the design space of diffusion-based generative models. In *advances in neural information processing systems (neurips)*, 2022.
- [34] Julia Kiessner et al. The tuh abnormal expansion eeg corpus (tuabex). *NeuroImage: Clinical*, 38:103317, 2023.

- [35] Kevin Kilgour, Mauricio Zuluaga, Umut Simsekli, Justin Salamon, Juan Pablo Bello, and Najim Dehak. frechet audio distance: a metric for evaluating music enhancement algorithms. *arxiv preprint arxiv:1812.08466*, 2019.
- [36] Diederik P Kingma and Jimmy Ba. Adam: A method for stochastic optimization. In *International Conference on Learning Representations*, 2015.
- [37] Guido Klein, Pierre Guetschel, Gianluigi Silvestri, and Michael Tangermann. Synthesizing eeg signals from event-related potential paradigms with conditional diffusion models. In *Proceedings of the 9th Graz Brain–Computer Interface Conference*, pages 438–443, 2024.
- [38] Zhifeng Kong, Wei Ping, Jiaji Huang, Kexin Zhao, and Bryan Catanzaro. diffwave: a versatile diffusion model for audio synthesis. *arxiv preprint arxiv:2009.09761*, 2020.
- [39] Tuomas Kynkäänniemi, Tero Karras, Samuli Laine, Jaakko Lehtinen, and Timo Aila. improved precision and recall metric for assessing generative models. In *advances in neural information processing systems (neurips)*, 2019.
- [40] Vernon J. Lawhern, Amelia J. Solon, Nicholas R. Waytowich, Shaun M. Gordon, Chou P. Hung, and Brent J. Lance. eegnet: a compact convolutional neural network for eeg-based brain–computer interfaces. *Journal of Neural Engineering*, 15(5):056013, 2018.
- [41] Lequan Lin, Zhengkun Li, Ruikun Li, Xuliang Li, and Junbin Gao. Diffusion models for time series applications: A survey. *arXiv preprint arXiv:2305.00624*, 2023.
- [42] Yaron Lipman, Ricky T. Q. Chen, Haggai Ben-Hamu, Maximilian Nickel, and Matthew Le. flow matching for generative modeling. *arxiv preprint arxiv:2210.02747*, 2022.
- [43] Yang Liu, Zhen Li, Pranay Kothari, Evangelos Theodorou, and Yang Song. flow straight and fast: learning to generate and transfer data with rectified flow. *arxiv preprint arxiv:2209.03003*, 2022.
- [44] David Lopez-Paz and Maxime Oquab. revisiting classifier two-sample tests. In *international conference on learning representations (iclr)*, 2017.
- [45] Ilya Loshchilov and Frank Hutter. Decoupled weight decay regularization. In *International Conference on Learning Representations*, 2019.
- [46] Tian-Jian Luo and Bin Lu. Eeg signal reconstruction using a generative adversarial network with a temporal–spatial–frequency loss. *Frontiers in Neuroinformatics*, 14:15, 2020.
- [47] Tomoya Matsumoto, Takayuki Miura, and Naoto Yanai. Membership inference attacks against diffusion models. *arXiv preprint arXiv:2302.03262*, 2023.
- [48] Leland McInnes, John Healy, and James Melville. UMAP: Uniform manifold approximation and projection for dimension reduction. *arXiv preprint arXiv:1802.03426*, 2018.
- [49] Takeru Miyato and Masanori Koyama. cGANs with projection discriminator. In *International Conference on Learning Representations*, 2018.
- [50] A. Mognon, J. Jovicich, L. Bruzzone, and M. Buiatti. Adjust: An automatic eeg artifact detector based on the joint use of spatial and temporal features. *Psychophysiology*, 48(2):229–240, 2011.
- [51] Chitra S. Nayak and Sandip Bandyopadhyay. mesial temporal lobe epilepsy. In *StatPearls*. StatPearls Publishing, Treasure Island (FL), 2023. [updated 2023 may 22; cited 2025 jan].
- [52] Cherif Neifar, Abdennaceur Kachouri, et al. diff-ecg: realistic electrocardiogram generation with diffusion probabilistic models. *arxiv preprint arxiv:2306.01875*, 2023.
- [53] Alexander Quinn Nichol and Prafulla Dhariwal. improved denoising diffusion probabilistic models. In *international conference on machine learning (icml)*, pages 8162–8171, 2021.
- [54] Hugh Nolan, Robert Whelan, and Richard B. Reilly. Faster: Fully automated statistical thresholding for eeg artifact rejection. *Journal of Neuroscience Methods*, 192(1):152–162, 2010.

- [55] Guido Nolte, Ou Bai, Lewis Wheaton, Zoltan Mari, Sherry Vorbach, and Mark Hallett. Identifying true brain interaction from eeg data using the imaginary part of coherency. *Clinical Neurophysiology*, 115(10):2292–2307, 2004.
- [56] Iyad Obeid and Joseph Picone. The temple university hospital eeg data corpus. *Frontiers in Neuroscience*, 2016.
- [57] Adam Paszke, Sam Gross, Francisco Massa, Adam Lerer, James Bradbury, Gregory Chanan, Trevor Killeen, Zeming Lin, Natalia Gimelshein, Luca Antiga, Alban Desmaison, Andreas K\"opf, Edward Yang, Zachary DeVito, Martin Raison, Alykhan Tejani, Sasank Chilamkurthy, Benoit Steiner, Lu Fang, Junjie Bai, and Soumith Chintala. Pytorch: An imperative style, high-performance deep learning library. In *Advances in Neural Information Processing Systems*, 2019.
- [58] Andreas Pedroni, Arman Bahreini, and Nicolas Langer. Automagic: Standardized preprocessing of big eeg data. *bioRxiv*, page 460469, 2019. Preprint.
- [59] William Peebles and Saining Xie. scalable diffusion models with transformers. In *international conference on machine learning (icml)*, 2023.
- [60] Wei Yan Peh, Yuanyuan Yao, and Justin Dauwels. Transformer convolutional neural networks for automated artifact detection in scalp eeg. *arXiv preprint arXiv:2208.02405*, 2022.
- [61] Ethan Perez, Florian Strub, Harm de Vries, Vincent Dumoulin, and Aaron Courville. film: visual reasoning with a general conditioning layer. In *aaai conference on artificial intelligence*, 2018.
- [62] Olaf Ronneberger, Philipp Fischer, and Thomas Brox. U-net: Convolutional networks for biomedical image segmentation. In *Medical Image Computing and Computer-Assisted Intervention (MICCAI)*, 2015.
- [63] Yannick Roy, Hubert Banville, Isabela Albuquerque, Alexandre Gramfort, Tiago H. Falk, and Jocelyn Faubert. Deep learning-based electroencephalography analysis: A systematic review. *Journal of Neural Engineering*, 16(5):051001, 2019.
- [64] Mehdi S. M. Sajjadi, Olivier Bachem, Mario Lucic, Olivier Bousquet, and Sylvain Gelly. Assessing generative models via precision and recall. In *Advances in Neural Information Processing Systems*, 2018.
- [65] Tim Salimans and Jonathan Ho. progressive distillation for fast sampling of diffusion models. *arxiv preprint arxiv:2202.00512*, 2022.
- [66] Robin Tibor Schirrmeister, Jost Tobias Springenberg, Lukas D. J. Fiederer, Martin Glasstetter, Katharina Eggersperger, Michael Tangermann, Frank Hutter, Wolfram Burgard, and Tonio Ball. Deep learning with convolutional neural networks for eeg decoding and visualization. *Human Brain Mapping*, 38(11):5391–5420, 2017.
- [67] Vinit Shah, Eva von Weltin, Silvia Lopez, James R. McHugh, Lily Veloso, Meysam Golmohammadi, Iyad Obeid, and Joseph Picone. The temple university hospital seizure detection corpus. *Frontiers in Neuroinformatics*, 12:83, 2018.
- [68] Jiaming Song, Chenlin Meng, and Stefano Ermon. Denoising diffusion implicit models. *arXiv preprint arXiv:2010.02502*, 2020.
- [69] Yang Song, Chenlin Meng, and Stefano Ermon. consistency models. *arxiv preprint arxiv:2303.01469*, 2023.
- [70] Yang Song, Jascha Sohl-Dickstein, Diederik P. Kingma, Abhishek Kumar, Stefano Ermon, and Ben Poole. Score-based generative modeling through stochastic differential equations. *arXiv preprint arXiv:2011.13456*, 2020.
- [71] Philipp Stenger, Paul Krueger, Jan Bauer, et al. evaluation measures for synthetic time series: a taxonomy and empirical study. *Journal of Big Data*, 11(1):92, 2024.

- [72] Muhang Tian, Bernie Chen, Allan Guo, Shiyi Jiang, and Anru R. Zhang. Reliable generation of privacy-preserving synthetic electronic health record time series via diffusion models. *arXiv*, 2024.
- [73] Giulio Tosato, Cesare M. Dalbagno, and Francesco Fumagalli. Eeg synthetic data generation using probabilistic diffusion models. *arXiv preprint arXiv:2303.06068*, 2023.
- [74] Jose Antonio Urigüen and Begoña García-Zapirain. EEG artifact removal—state-of-the-art and guidelines. *Journal of Neural Engineering*, 12(3):031001, jun 2015.
- [75] Laurens van der Maaten and Geoffrey Hinton. Visualizing data using t-SNE. *Journal of Machine Learning Research*, 9:2579–2605, 2008.
- [76] Julius Vetter, Richard Gao, and Jakob H. Macke. Generating realistic neurophysiological time series with denoising diffusion probabilistic models. *Patterns*, 5(9):101047, 2024.
- [77] Peter D. Welch. the use of fast fourier transform for the estimation of power spectra: a method based on time averaging over short, modified periodograms. *IEEE Transactions on Audio and Electroacoustics*, 15(2):70–73, 1967.
- [78] Yuxin Wen, Shaofei Li, Micah Goldblum, Avi Schwarzschild, Wojciech Czaja, and Tom Goldstein. tree-ring watermarks: fingerprinting deep generative models. *arxiv preprint arxiv:2305.20030*, 2023.
- [79] Irene Winkler, Stefan Haufe, and Michael Tangermann. Automatic classification of artifactual ica-components for artifact removal in eeg signals. *Behavioral and Brain Functions*, 7(30):1–15, 2011.
- [80] Ryuichi Yamamoto, Eunwoo Song, and Jae-Min Kim. parallel wavegan: a fast waveform generation model based on generative adversarial networks with multi-resolution spectrogram. *ieee/acm transactions on audio, speech, and language processing*, 28:1837–1847, 2020.
- [81] Jinsung Yoon, Daniel Jarrett, and Mihaela van der Schaar. Time-series generative adversarial networks. In *Advances in Neural Information Processing Systems*, volume 32, 2019.
- [82] Lvmin Zhang, Anyi Rao, and Maneesh Agrawala. adding conditional control to text-to-image diffusion models. *arxiv preprint arxiv:2302.05543*, 2023.

A Appendices and Supplementary Material

A.1 Compute & Environment

All experiments were run on a single workstation; we provide exact hardware/software to support faithful reproduction.

- **Hardware.** AMD Ryzen-class desktop (32 logical cores), 96 GB system RAM, 2 TB NVMe SSD, single NVIDIA RTX 4080 (16 GB). No multi-GPU or distributed training was used.
- **OS / Software Stack.** Pop!_OS 22.04 LTS (Linux kernel 6.x), Python 3.12, PyTorch 2.2 with CUDA 12.1 toolchain, cuDNN 9, NumPy, SciPy, and scikit-learn (feature metrics / classifiers). Reproducibility scripts pin package versions in `requirements.txt`.
- **Diffusion (DDPM) model.** 1D U-Net with FiLM conditioning: channel widths (64, 128, 256), down/up depth 3, residual blocks with GroupNorm, sinusoidal timestep embedding fused with a learned class embedding (dim 13 including a null token for classifier-free guidance). EMA of model weights (decay 0.999) maintained for sampling.
- **GAN (WGAN-GP) model.** Transposed-convolution generator (latent $z \sim \mathcal{N}(0, I_{128})$) concatenated with one-hot class vector) with channel progression (128, 128, 64, 32, C); projection discriminator with mirrored strides and learned class embedding (dim 128). Optional STFT L_1 spectral auxiliary loss (disabled unless stated).
- **Optimization.** WGAN-GP: Adam ($\beta_1=0.5, \beta_2=0.9$), batch 256, critic steps $n_{\text{critic}}=5$, gradient penalty $\lambda_{gp}=10$. Diffusion: AdamW ($\beta_1=0.9, \beta_2=0.999$, weight decay 10^{-4}), linear β schedule with $T=1000$ training steps, sampling with 80-step deterministic DDIM-style schedule and classifier-free guidance scale 1.5.
- **Data pipeline.** Host-side prefetch and pinned memory enabled; each training window is $C=8$ channels with length 250 (WGAN-GP) or 500 (DDPM). GAN inputs are per-window min-max scaled to $[-1, 1]$; diffusion inputs are per-recording z -scored per channel.
- **Sampling.** For quantitative evaluation we draw $N=3000$ windows per artifact class (5 classes) using EMA weights for diffusion and the best-FID checkpoint for WGAN-GP. Guidance (CFG) applied only in diffusion sampling; scale tuned on validation FID (best at 1.5).
- **Artifacts covered.** Five classes: muscle, eye, electrode, chewing, shiver. A “none” (clean) label is excluded from training to focus model capacity on artifact morphology.
- **Runtime.** Per-epoch wall-clock: WGAN-GP 2.1 min, DDPM 3.4 min. Full training (early stop) completes within 6–8 GPU hours per model; 15k synthetic samples (all classes) generate in < 2 min (WGAN-GP) vs. 6 min (DDPM 80 steps).
- **Determinism.** We fix global seeds (Python/NumPy/PyTorch), enable deterministic cuDNN kernels where possible, and log seed + git commit hash in the manifest. Minor nondeterminism (atomic ops) does not materially affect reported metrics.

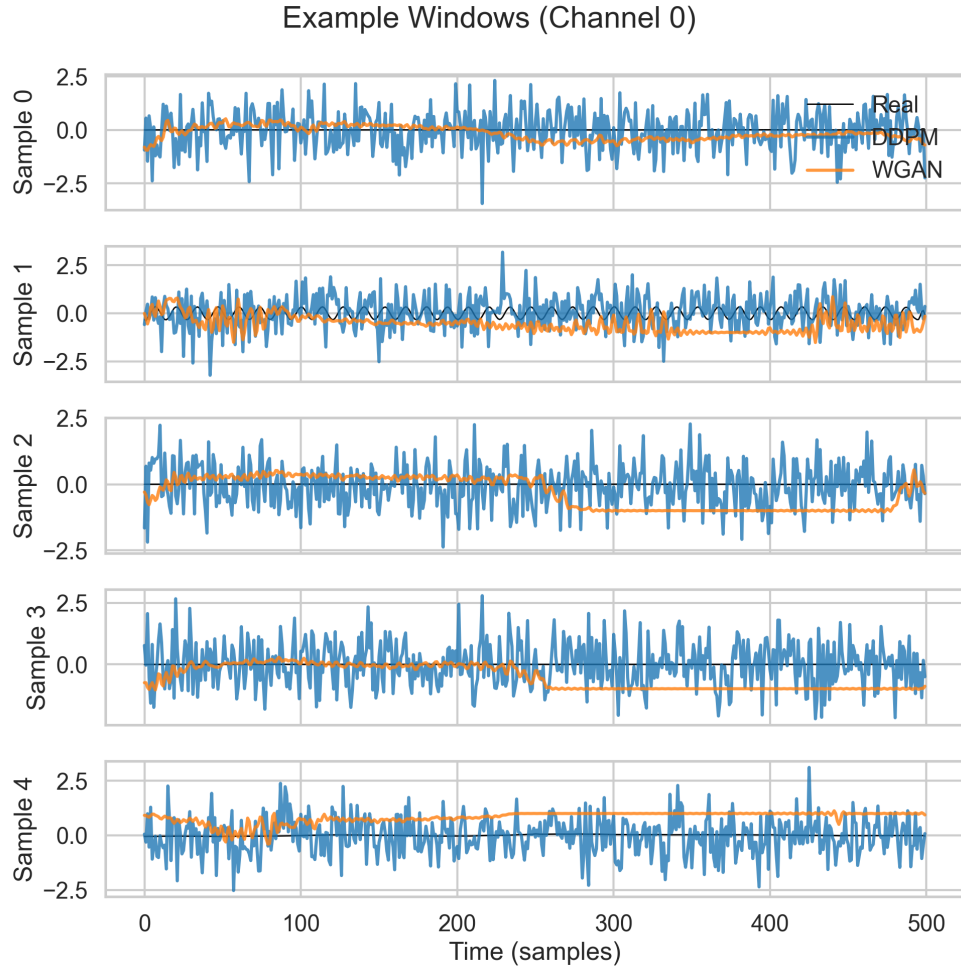


Figure 3: Additional qualitative example of the shiver class. Multi-channel windows highlighting morphology variety across artifacts beyond the main-text panel.

A.2 Additional Figures

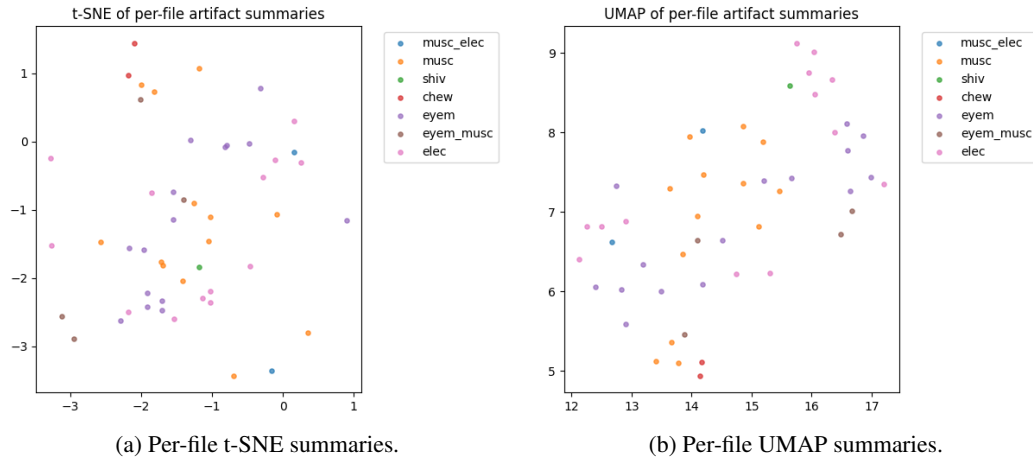


Figure 4: Per-file embedding summaries. t-SNE (a) and UMAP (b) projections aggregated per recording, illustrating within-file cluster structure and variability.

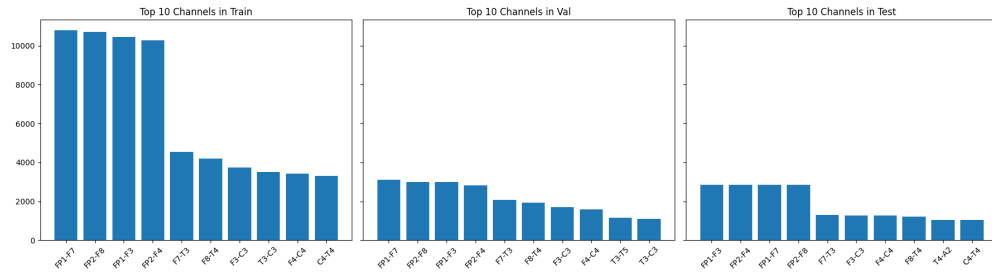


Figure 5: Channel distribution per split (multilabel). Relative presence of channels across train/val/test, useful for confirming split balance and avoiding channel leakage.

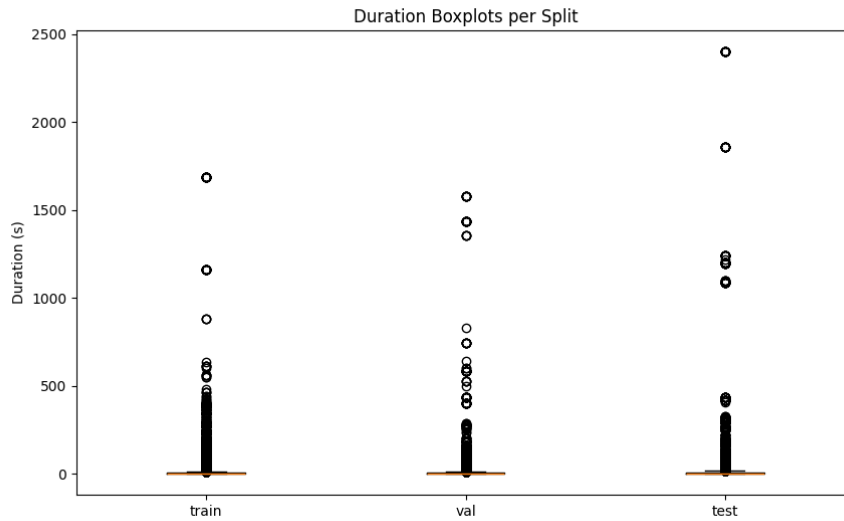


Figure 6: Window duration statistics by artifact (multilabel). Boxplots summarize duration dispersion, complementing main-text descriptive stats.